Analytical and Bioanalytical Chemistry
https://doi.org/10.1007/s00216-025-05958-1

RESEARCH PAPER

Evaluation of fused deposition modeling (FDM)-printed devices for microfluidic-based cell culture studies

Samuel Azibere[1] · Michael Borovik[2,3] · Andrew F. Hall[2,3] · Scott A. Sell[2,3] · R. Scott Martin[1,3]

Received: 11 April 2025 / Revised: 28 May 2025 / Accepted: 3 June 2025

Abstract

In this paper, we undertook an in-depth investigation of the parameters that can be optimized to create FDM-based devices (both static and fluidic) that are leak-free and can be used for cell culture. Two different types of FDM printers (Stratasys Fortus 250mc and Bambu Lab P1S/X1-carbon) were utilized and devices were printed with a polystyrene filament, since this polymer is commonly used to make cell culture flasks. Stratasys-printed devices were made leak-free by increasing the negative "air gap" values to offset the toolpath, which significantly minimized voids between layers. Bambu Lab-based devices exhibited no leakage when printed with the ironing variable enabled. These parameters were optimized based on the design (static vs. fluidic), and the final devices were able to withstand leakage when subjected to flow experiments. It was found that these devices led to the successful culture of bovine pulmonary artery endothelial cells and Madin-Darby canine kidney cells, and a comparison was made to culturing these cells on a PolyJet-based device (printed with VeroClear material). NMR analysis was employed to determine if any potential leachates of polystyrene resulted after printing of the devices. Finally, fiber scaffolds were integrated into devices to mimic extracellular matrix (ECM) and to demonstrate the ability to perform cell culture under flow conditions in such devices. It is clear that with the developed settings, robust fluidic devices for cell culture can be created and used for the successful culture of endothelial and epithelial cells.

Keywords Microfluidics/microfabrication · Bioanalytical methods · Cell systems/single cell analysis · 3D printing

Introduction

The use of microfluidic devices for in vitro cell culture studies has become increasingly popular due to the ability of the devices to provide continuous nutrient supply, facilitate waste removal, introduce shear stress, and integrate analytical measurement schemes [1–5]. Various approaches have been used to fabricate such devices. Soft lithography with poly(dimethylsiloxane) (PDMS) has been a popular approach; however, in recent years, 3D printing has emerged as a viable alternative for producing these devices. This is due to the ability of this technique to batch print complex, 3-dimensional devices at once, to print devices with different materials and compositions, to easily share CAD designs, and to integrate real-world interconnects (fittings, tubing, etc.) [6]. Several techniques are available to be used to perform 3D printing, with the majority of fluidic devices fabricated using fused deposition modeling (FDM, with materials such as acrylonitrile butadiene styrene, polystyrene or polycarbonate), some form of stereolithography (SLA) or digital light processing (DLP, each with acrylate or epoxide-based materials), or MultiJet/PolyJet printing (ink-jet type process using acrylate-based materials and photoinitiators) [6–9].

FDM printing uses a thermoplastic filament material that is extruded through a nozzle that is heated so that the material is above its glass transition temperature, causing the material to liquefy and flow. The nozzle can deposit this material on one layer in an x–y fashion, after which the layer cools and resolidifies. The stage then moves in the z-direction to start printing the next layer. As each new layer builds upon the previously extruded layer, the semi-liquid forms bonds to the preceding layer [9–11]. There are many materials available for FDM printing, including polylactic

✉ R. Scott Martin
scott.martin@slu.edu

[1] Department of Chemistry, Saint Louis University, 3501 Laclede Ave, St. Louis, MO 63103, USA

[2] Department of Biomedical Engineering, Saint Louis University, St. Louis, USA

[3] Center for Additive Manufacturing, Saint Louis University, St. Louis, USA

Published online: 20 June 2025

acid (PLA) [12], acrylonitrile butadiene styrene (ABS) [13], and polycarbonate (PC) [14]. Despite being a reliable, user-friendly, and inexpensive technique, when using standard print conditions, significant limitations exist with fabricating optically transparent and void-free devices. These voids can cause leaking between layers in fluidic devices [15]. For most FDM printers, resolution is around 125 µm in the x–y direction and 200 µm in the z direction [6]. More recently, smaller nozzles have been used to produce microfluidic devices with channel sizes less than 100 µm [16, 17].

Recent studies have revealed the significant potential of 3D-printed devices in advancing cell culture studies [18–21]. Several different approaches and printing methods have been used to make these devices. Examples include PolyJet-printed devices from VeroClear and MED610 resins with embedded scaffolds for epithelial/endothelial cell culture [3], a SLA-based perfusion device for culturing multicellular spheroids [22], PolyJet-printed devices designed to accommodate transwell inserts for drug transport studies [23], a microfluidic blood–brain barrier (BBB) model utilizing VeroClear material [24], and a PolyJet-printed device with collagen scaffolds for cell culture, enabling transepithelial and transendothelial electrical resistance (TEER) measurements [25].

There have been some concerns raised regarding the biocompatibility of 3D printing materials used in cell culture studies, with several reports on this issue. To date, most of the devices for cell culture have used SLA, DLP, or PolyJet printing; therefore, studies on biocompatibility have focused on these techniques. In particular, these studies have sought to investigate any leaching of materials over time due to incomplete polymerization of photoreactive resins [20]. A study conducted with PolyJet printing of MED610 found that a thorough cleaning procedure, including sonication with isopropanol, led to the successful culture of primary mouse myoblasts [26]. In another study, the effect of PolyJet-printed materials (Vero-clear or MED610) and cleaning methods on culturing 2 cell lines was investigated [3]. Bovine pulmonary artery endothelial cells (BPAECs) and Madin-Darby canine kidney (MDCK) cells were directly cultured on devices that underwent various treatment/cleaning methodologies, such as sodium hydroxide/sodium metasilicate solution. Compared to cells cultured on untreated devices, results indicated cells cultured on treated devices showed characteristics similar to what is obtained in traditional culture flasks, and LC–MS/MS analysis was used to determine potential leachates from untreated devices [3]. Rimington et al. used devices from 3 different 3D printing techniques (SLA, PolyJet, and laser sintering) to culture several cell lines [27]. Prior to culturing cells, devices were cleaned with isopropanol and methylated spirits. Results of the study showed a mixture of compatibility for each cell type when cultured on the different printed parts. For example, VeroClear (PolyJet printing) devices were found to support proliferation of skeletal muscle cells and differentiation for neuronal cells, but such devices had no compatibility with hepatic cells. The authors employed FT-IR and NMR spectroscopy to identify bands correlating with uncured acrylate materials in the leachate [27]. In addition, a number of studies have provided evidence of the use of coatings to improve the biocompatibility of devices [19, 28, 29]. With the aforementioned studies, both the specific printing method and the cell type must be taken into account when investigating the effectiveness of culturing cells on 3D-printed devices.

Here, we perform an in-depth investigation of the parameters that can be changed to create FDM-based microfluidic devices that are leak-free and can be used for cell culture. Two different printers were utilized. Devices were printed with polystyrene (PS) filament, as this polymer is commonly used to make cell culture flasks. Importantly, fluidic devices that could withstand flow experiments resulted from these studies, and the devices were used to culture two different cell lines under both static and flow conditions. NMR analysis was employed to determine if any potential leachates of polystyrene result after printing of the devices. Electrospun fiber scaffolds were also incorporated into the fluidic devices to enable flow-based cell culture studies. A detailed comparison was made between the FDM-printed devices and devices with the same design printed with PolyJet technology using VeroClear material. It is clear that with the developed settings, robust fluidic devices for cell culture can be created and used for the successful culture of endothelial and epithelial cells.

Experimental

Materials

High-impact polystyrene materials were obtained from Gizmo Dorks (Gizmo Dorks LLC, Temple City, CA) and Matter Hackers (Lake Forest, CA). 1/4–28 Brass Heat Set Inserts were obtained from McMaster-Carr (McMaster-Carr, Elmhurst, IL). Tygon tubing (508 mm i.d.) was obtained from Cole-Parmer. Fittings (Idex P-202) were obtained from IDEX Health & Science (Oak Harbor, WA). Polystyrene pellets (280 kDa M.W.), Rhodamine B, tetrabutylammonium bromide, and deuterated chloroform were all obtained from Millipore Sigma (St. Louis, MO).

3D printing

Two different printer types were used in this study: Stratasys Fortus 250mc and Bambu Lab printer (P1S or X1-Carbon). High-Impact Polystyrene (HIPS) filament in "Natural" color

was used to print devices. Two different designs were completed in SolidWorks 2022 (Fig. S1). One of the designs had the same dimensions as a 35-mm culture dish (Eppendorf, Hamburg, Germany) in order to make a direct comparison for static culture studies (depth 2.0 mm, diameter 35 mm). The other design is an insert-based flow device that can accommodate an insert containing nanofibers [4, 30]. This fluidic device assumes placement of 1/4–28 Heat Set Inserts on either side, allowing the connection of commercially available fittings and tubing (Fig. S2) [31]. Stratasys Fortus 250mc settings are applicable to printers that are supported by the Stratasys Insight slicing program. The Bambu printer settings are applicable to any FDM printer that is supported by slicing programs such as Prusa Slicer, Bambu Studio, and Ultimaker Cura.

Stratasys Fortus 250mc print settings

The printer has dual heads, and HIPS was printed from the support nozzle, as the nozzle has a larger orifice diameter to prevent clogging. A 0.40-mm diameter nozzle with a layer height of 0.254 mm was used to print devices. The flow devices were designed and processed to prevent support structures printing inside of the channels.

To optimize the printer for leak-free devices, the toolpath of the parts was modified to have a negative "air gap" offset (applied to all applicable contour/raster combinations). This effectively forces the printer to overlap adjacent beads of material, creating an overflow that fills the voids that would otherwise exist. While standard print settings of the printer have an air gap of 0.0 mm, here the static devices were printed with air gaps of − 0.0254 and − 0.0508 mm, respectively. These air gaps, including − 0.0762 mm, were also used to print the flow devices. Printing with varying air gap values was also tested for the flow devices, where, for example, a small section (at least 2 layers) around the channel was printed with a − 0.0254 mm air gap and the remaining bulk printed with − 0.0508 mm (in order to prevent channel deformation). Heat set inserts were installed in FDM-printed devices to allow the connection of tubing from devices to a pump. To install the heat set inserts, a custom-built machine from a discarded FDM printer was used to transfer heat from a heated conical dowel to the brass heat set inserts after gently inserting them on either side of the device. Upon pressing down the handle of the machine (to apply pressure), the heat set melts/inserts into device material, forcing the material to reflow around heat sets into the device (see Fig. S2 for a detailed description of the process).

Bambu Lab print settings

Devices were printed using a Bambu Lab PS1 or X1-Carbon printer with a 0.40-mm nozzle and a 0.20-mm layer height. Bambu Lab printers utilized Bambu Studio slicer software for print settings. This slicer has a flow ratio (Extrusion Multiplier) parameter typically expressed in percentage, which is 100% by default. As part of the toolpath generation, the slicer calculates the amount of material needed to be extruded via the nozzle in volume/time (mm^3/s). The calculation is based on the bead width (related to nozzle orifice), bead height (defined by layer height) and travel speed. To print devices with standard printing settings in this study, the flow ratio was set to 100% for both static and flow devices. The flow devices were designed and processed to prevent support structures from printing in the channel.

The printer settings were optimized by enabling the "ironing" feature for all solid layers. Ironing is the retracing of the toolpath with a minimum amount of material being dispensed (with the amount of material being a percentage of the original flow ratio). As described in the results/discussion, this process reduces the size of any available voids in the devices. Using this approach, devices were printed with 0% "ironing flow." The ironing flow % was then varied to print devices with an ironing flow of 2.5, 5, and 10%, respectively.

PolyJet 3D printing

Stratasys J735 PolyJet printer with VeroClear model material was utilized to print both static and flow devices using the designs described earlier. This was necessary so that we could perform a comparison study between the FDM-printed PS and the PolyJet-printed VeroClear materials with regard to cell culture. Standard high-quality print settings were used to print the devices. Static culture devices were printed with no support material in the voids. Only the carpet layer included support material (this was removed before use). For the flow devices, the printer was made to print support material in the channel of the devices. All devices (static and flow devices) were manually cleaned of the support material by placing them in sodium hydroxide/sodium metasilicate bath overnight followed by thorough rinsing with DI water before use as previously reported by Currens et al. [3].

Leakage test

Leaking studies were performed on devices by pipetting 3 mL of red food dye solution into the static culture devices and placing them in an incubator overnight (37 °C). The flow devices were connected to a peristaltic pump (Gilson Minipuls 2, France) that circulated 1 mM of rhodamine B through the channel at 15 µL/min for 1 h. A syringe pump equipped with a 2.5-mL syringe of rhodamine B was also used to test leakage. The flow devices were dissected using a bandsaw or CNC milling machine (LDO Millennium Machines Milo v1.5, MatterHackers, CA) and examined

with a stereo microscope (Olympus SZ61, Tokyo, Japan). It should be noted that using the milling machine to dissect the devices had a very small impact on the determined channel size. As can be seen in Fig. S3, where a 1.0-mm hole was drilled into a printed piece of PS, after milling, the channel size is slightly smaller (0.972 mm). Since this technique was to look at relative changes in size for different print parameters, this amount of difference is tolerable. Studies involving the measurement of pressure as a function of flow rate utilized a Shimadzu LC-10AT VP HPLC pump.

Cell culture under static conditions

Bovine pulmonary artery endothelial cells (BPAECs, Cell Applications, San Diego, CA), between passages 3 and 7, were cultured in T-75 flasks (Corning, NY) using high-glucose Dulbecco's modified Eagle's medium (DMEM, ATCC, Manassas, VA) containing 10% FBS (Millipore Sigma, St. Louis, MO) and 1% penicillin–streptomycin (Lonza, Walkersville, MD). Cells were cultured at 37 °C and 5% CO_2, and media were exchanged every 72 h until 80% confluence was achieved. Cells were passaged with the aid of a trypsin–EDTA solution (Millipore Sigma, St. Louis, MO). Seeding density was determined after counting cells using a cell hemocytometer. Cells were seeded in FDM 3D-printed static devices (35 mm diameter device) at ~ 2×10^4 cells per mm^2. Prior to cell seeding, the 3D-printed devices were coated with a 100 µg/mL fibronectin solution (with exact concentration being optimized) to improve the adhesion of the cells to the device surface. Cells were placed in an incubator and monitored for 2, 24, and 48 h. In a similar experiment, the same seeding density of cells was cultured in PolyJet 3D-printed devices for a comparative analysis between print technologies. For each of the printing technologies, three devices were utilized for the cell culture studies.

Madin-Darby canine kidney cells (MDCK NBL-2, ATCC, Manassas, VA) between passages 10–14 were cultured in T-75 flasks (Corning, NY) using Eagle's Minimum Essential Medium (EMEM, Millipore Sigma, St. Louis, MO) containing 10% FBS and 1% penicillin–streptomycin. Cell media was changed every 72 h until confluency was achieved. Cells were cultured and passaged in conditions similar to subculturing for BPAECs. Cells were seeded in both FDM and PolyJet 3D-printed static devices at ~ 1.7×10^4 cells per mm^2. Cells were incubated and monitored over 2, 24, and 48 h. The 3D-printed devices were coated with a 100 µg/mL fibronectin solution before seeding the cells.

3D cell culture with flow

Fibrous scaffolds were electrospun and embedded in the cell culture devices to investigate their effect in 3D cell culture. Polystyrene nanofibers with average sizes ranging between 200 and 400 nm were prepared via electrospinning [3, 32]. A 12% (w/v) polystyrene solution was prepared by dissolving polystyrene pellets and 1% tetrabutylammonium bromide in dimethylformamide (DMF). The solution was allowed to completely dissolve by placing it on a shaker overnight. A pressure of 4 psi was then applied (using helium gas) to a glass vial with a septum containing about 2 mL of the dissolved polystyrene solution to induce flow through a 15-cm, 150-µm-I.D. fused silica capillary. High voltage between 15 and 17 kV was applied to the solution via a platinum wire (0.5 mm diameter; Alfa Aesar, Ward Hill, MA) connection through the septum. The electrospinning setup was located in a customized plexiglass chamber. The optimal temperature and humidity conditions for electrospinning polystyrene fibers were found to be 22 °C and less than 40%, respectively. This solution was electrospun on a 10 cm × 18.5 cm sheet of Whatman lens cleaning tissue (Grade 105; GE Healthcare Life Sciences, Marlborough, MA). This sheet was wrapped around a grounded mandrel (14 cm long by 6 cm in diameter) that rotated at 300 rpm and would slide horizontally over a 12-cm span at 6 cm/s. After 90 min of spinning, fibers were collected and characterized using scanning electron microscopy (SEM).

Fibers were peeled from the lens paper and gently transferred onto a polystyrene sheet. This sheet was laser cut to create rectangular fibrous inserts with dimensions 2.8 mm × 17.2 mm, with this size fitting insert-based flow devices from both FDM and PolyJet printing technologies [4]. To adhere cells before they were placed in the device, the fiber-coated inserts were secured on the bottom of a 40-mm petri dish by use of double-sided tape. Inserts were rinsed with PBS three times, followed by a final rinse using deionized (DI) water and air-dried overnight. Inserts were plasma treated for 30 s at medium RF before being coated with 100 µg/mL fibronectin solution and allowed to dry prior to cell culture. A confluent T-75 flask of BPAECs was detached by trypsin, which was then centrifuged and re-suspended in fresh warm media. Cells were seeded by dispensing 40 µL of the cell suspension (~ 3×10^5 cells) onto each fibronectin coated insert and incubated for ~ 2 h, after which 3 mL of fresh warm media was added to the petri dish and incubated for 24 h. The media was removed, and the inserts were placed into the slots in the flow devices (FDM vs. PolyJet) with tweezers and immediately connected to a peristaltic pump via threaded ports in the device (heat set insert for FDM devices and printed threads for PolyJet devices). The peristaltic pump circulated media through the devices while in the incubator at 15 µL/min for 24 h. Inserts were removed from the flow devices, rinsed three times with PBS, and incubated with acridine orange staining solution for 5 min. Inserts were rinsed with PBS and imaged via a Leica SP8 confocal microscope.

NMR spectroscopy analysis of leachates

Leachates from the FDM 3D-printed devices were investigated using ^{1}H NMR (400 and 700 MHz, Bruker) by observing bands correlating to the aromatic ring of polystyrene. The 3D-printed cell culture (static) devices were rinsed with deionized water, followed by pipetting 3 mL 1× PBS into the devices. The devices were incubated at 37 °C and 5% CO_2 for 48 h before liquid–liquid extraction was carried out using the PBS sample and methylene chloride, followed by evaporation to concentrate the extract to a minimal volume. The extract was reconstituted in 1 mL deuterated chloroform for analysis. NMR spectra obtained were processed and analyzed using TopSpin and MestreNova software. Analysis was performed with 3 different devices.

In addition, a calibration curve was performed by preparing a 1 mg/mL stock solution of polystyrene, which was made by dissolving polystyrene (HIPS, same filament that was used for printing the devices) in deuterated chloroform (chloroform-d). The stock solution was allowed to completely dissolve by placing it on a shaker for 4 h. The solution was then diluted into standards with concentrations ranging from 50 to 250 µg/mL. These standards were analyzed, and the absolute integrals of the spectra obtained were used to generate the calibration curve. A recovery experiment was also conducted where the 1× PBS (10 mL) was spiked with 150 µg/mL (1 mL) of the polystyrene solution. Liquid–liquid extraction was performed following the aforementioned protocol.

Cell imaging

Cells were rinsed with 1 mL of 1X phosphate-buffered saline (pH = 7.0, Cytiva, Marlborough, MA) after 24 h of incubation in 3D-printed static devices. The cell inserts in flow devices were removed from the device after 24 h and rinsed in a similar manner. Both BPAECs and MDCK cells were stained with 100 µM acridine orange (Millipore Sigma, St. Louis, MO) for fluorescent imaging (after 5-min incubation), followed by another rinse with 1 mL of 1× PBS. Fluorescent images were obtained of cells directly on the devices and inserts using a Leica SP8 confocal microscope (with 10 × objective). Images were processed using the manufacturer's software (Leica Application Suite X) and further analyzed using FIJI/ImageJ.

Surface topography analysis

An FEI Inspect F50 (Lausanne, Switzerland) scanning electron microscope was used to evaluate voids in between the printed layers. For SEM analysis, samples of devices were dissected and sputter coated with gold (Desk V Standard Sputter Coater, Denton Vacuum LLC, Moorestown, NJ) before imaging. Images were captured and analyzed using ImageJ software to determine the average area of voids in printed models from both printers. Additionally, the electrospun nanofibers were also analyzed following this approach, and the average sizes of fibers were determined. Surface topography of the static devices printed using Bambu Lab printer was verified by performing 3D microscopic measurements using a VK-9700 3D laser scanning microscope (Keyence Corporation, Japan).

Cell viability assays

Cell viability was investigated by performing a viability assay using 3-(4,5-dimethylthiazol-2-Yl)−2,5-diphenyltetrazolium bromide (MTT; Millipore Sigma, St. Louis, MO). Cells were cultured on both FDM and PolyJet 3D-printed static devices for 24 h and 48 h, respectively, before adding the MTT reagents and lysing according to the manufacturer's protocol [33, 34]. In each comparison, a 2-h culture of cells with the same material/device type served as the control, allowing the absorbance of the 24- and 48-h cultures to be measured and normalized in relation to that of the 2-h time point. A MTT assay was also done directly on inserts for cells that were exposed to flow conditions for 24-h. The MTT assay was performed on BPAECs and MDCK cells. Samples were transferred to a 96-well plate to measure absorption at 550 nm using a plate reader (SpectraMax iD3, Molecular Devices). Cell viability using the MTT kit was done by normalizing the resulting absorption values to cells cultured for 2 h in the same material type serving as the control (to see if cells grew relative to the 2-h time point).

Results and discussion

FDM printing is based on the extrusion of thermoplastic filaments through a heated nozzle in a layer-by-layer process until the desired 3D object is created. While the printers and devices can be relatively inexpensive compared to other printing approaches, a significant limitation is the inability to print devices with minimum voids with default settings, even when printed at 100% (solid) infill. Due to various factors such as bead shrinkage, surface finish requirements, or surface tension, the beads deposited during the printing process are not square in their cross-section; rather, they are oval or slot-shaped, creating continuous "air gaps" (voids) throughout the model (see schematic in Fig. 1). In this study, various FDM 3D printers, including Stratasys Fortus 250mc and Bambu Lab printers (P1S and X1-Carbon), were used to print dish-like culture (static) and flow devices using polystyrene materials. Polystyrene is widely recognized as a material used in cell culture flasks. It is available for 3D

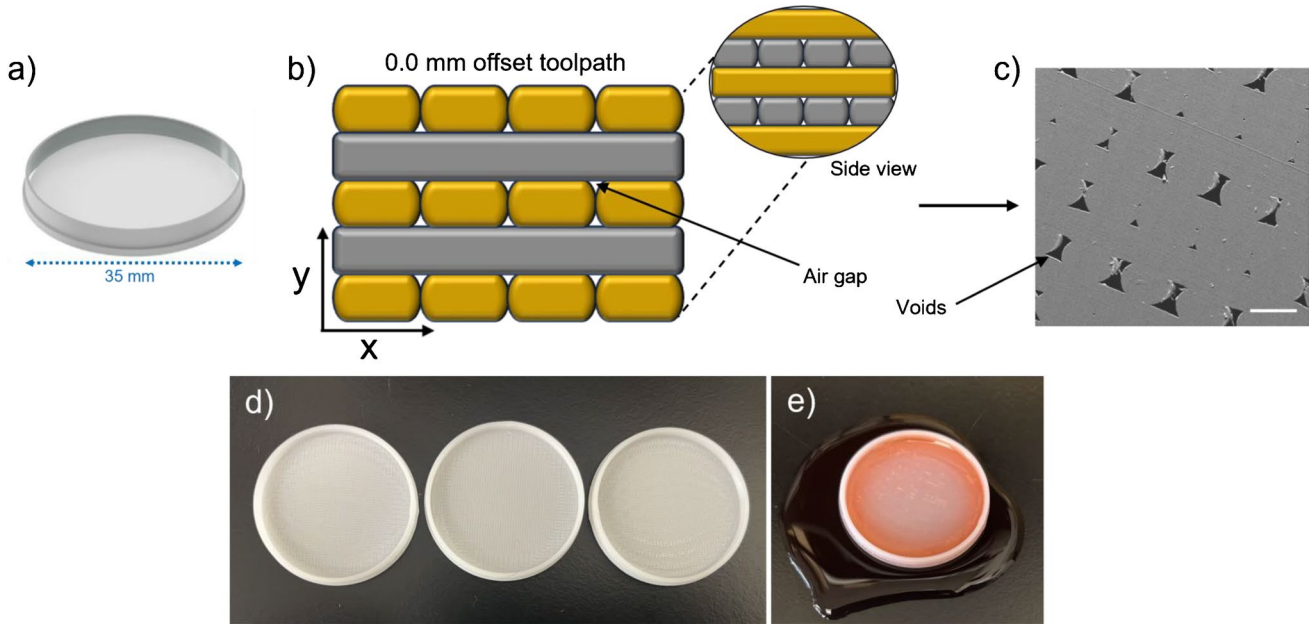

Fig. 1 Initial 3D-printed static devices using Stratasys FDM printing approach. **a** CAD rendering of FDM 3D-printed culture dish, based on dimensions of a 35-mm petri dish. **b** Illustration of regular toolpath with air gap 0.0 mm for standard printing. **c** SEM micrograph showing air gap voids between layers. **d** Printed devices in polystyrene (PS) materials. **e** Photograph showing printed device leaking when testing with red dye. Scale bar = 400 µm

printing as High-Impact Polystyrene (HIPS) filament. The static devices were designed to have the same dimensions as a 35-mm culture dish (Fig. 1a). The flow devices were designed to feature an insert-based device capable of accommodating one insert with cultured cells (see Fig. S1 for CAD designs).

Static devices printed with Stratasys Fortus 250mc

To print devices with the Stratasys Fortus 250mc, a spool of HIPS filament was loaded into the support material bay of the printer, and the T16-SRT30 support tip was used. This nozzle has a nominal orifice diameter of 0.40 mm and was utilized in place of the model tip T14 nozzle (0.36 mm diameter) to prevent clogging of the nozzle. The part was processed in Insight slicer software to print with the material in the support bay. The ABS build sheet installed in the printer was replaced with a polyetherimide (PEI) sheet with an adhesive coating since the HIPS material does not bind well to the ABS build sheets. The layer height was set to a default of 0.254 mm, and the bead width was set to a default of 0.508 mm. With these standard settings, static culture devices were printed (Fig. 1d) and tested via filling devices with a solution of red dye after overnight incubation. The results showed that these devices were not leak-free and leaked profusely between layers (Fig. 1e). The nature of the voids was verified by dissecting the devices using a milling machine (see "Experimental" and Fig. S3 for more information), and SEM micrographs (sample in Fig. 1c) were captured, processed, and analyzed using ImageJ software. Results showed that these standard printed devices exhibited a void density of 4 void/mm^2, with the average void area being 11,094 µm^2.

To optimize the printer for leak-free devices, the toolpath of the parts was modified to have a negative "air gap" offset applied to all applicable contour/raster combinations. This effectively forces the printer to overlap adjacent beads of material, creating an overflow that fills the voids. While the standard print setting (described above) has an air gap of 0.0 mm, here, the static devices were printed with air gaps of −0.0254 mm and −0.0508 mm, as illustrated in Fig. 2a and d. Devices printed with −0.0254 mm air gap were found to be unsuccessful (Fig. 2c); conversely, those with −0.0508 mm air gap resulted in devices that did not leak when tested, as shown in Fig. 2f. Voids in these devices were verified with SEM following the aforementioned dissection protocol (Fig. 2b and e). Comparatively, devices printed with an air gap of −0.0254 mm resulted in a void density of 3 void/mm^2 with the average void area being 4332 µm^2, while devices with −0.0508 mm air gap value had a void density of 1 void/mm^2 and an average void area of 1678 µm^2. These void areas indicated that the standard printed devices yielded at least 2.5 times the size of voids in devices with negative air gap values (see Fig. S4a for a graph that compares these values).

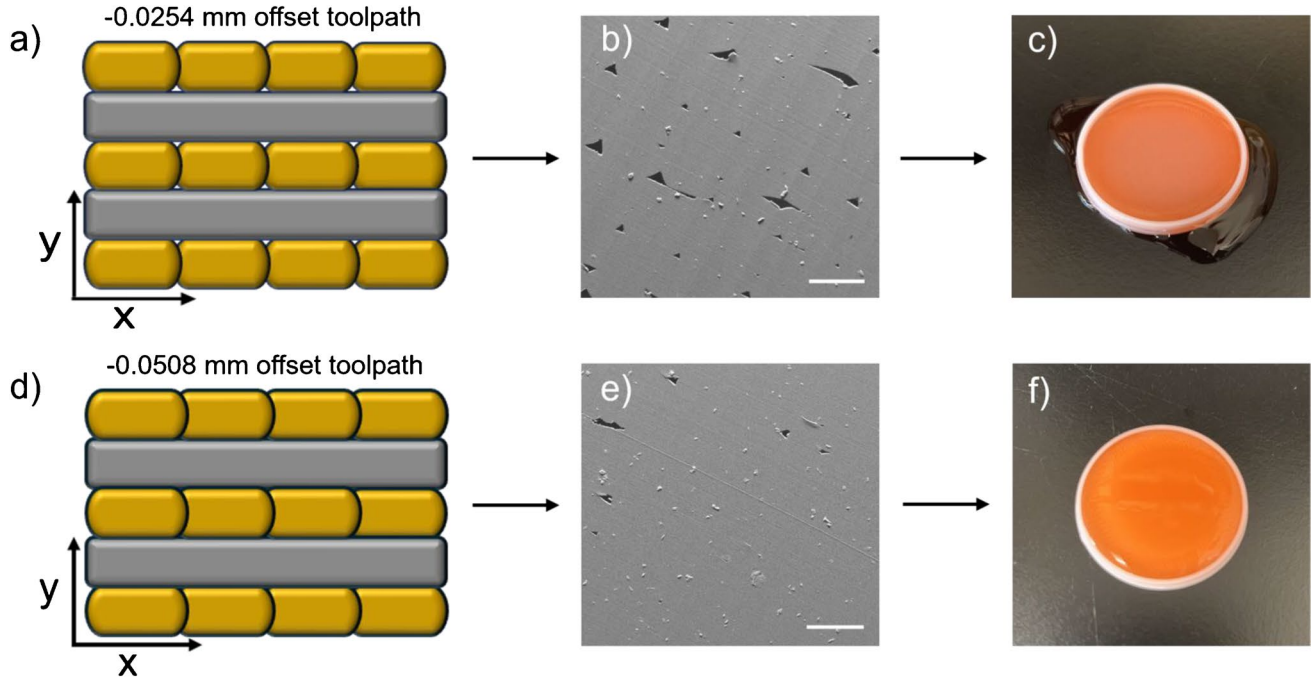

Fig. 2 Optimizing Stratasys printing parameters via offsetting toolpath to decrease air gap. **a** Illustration of offset toolpath with air gap −0.0254 mm. **b** SEM image showing voids (−0.0254 mm) between layers. **c** Photograph of printed devices (with −0.0254 mm air gap) leaking when tested with red dye. **d** Illustration of offset toolpath with air gap −0.0508 mm. **e** SEM image showing voids (−0.0508 mm) between layers. **f** Photograph of leak-free printed devices using air gap − 0.0508 mm. Scale bar = 400 µm

Static devices printed with Bambu Lab

The Bambu Lab FDM printers have several variables that can be adjusted, including temperature, flow rate, and ironing. It is common to modify the "flow ratio" in order to attempt printing leak-free devices. The standard flow ratio is typically 100%, and increasing the flow ratio (depending on the geometry of the design) can lead to over-extrusion, which is likely to minimize the number and size of voids between layers. However, in our studies, this method resulted in a poor surface finish. Therefore, a 100% flow ratio was used in these studies. As mentioned in the experimental section, this is a calculated value, where the slicer calculates the amount of material that needs to be extruded in volume/time.

One interesting feature of these printers is the "ironing" variable, which commands the printer to retrace the previous toolpath with a minimum deposition of material. This helps to expel any voids in the previous layer. For example, standard toolpath prints with a 100% flow of material and with an ironing value of 5% direct the printer to "iron" the toolpath, with the nozzle retracing the previous toolpath and delivering 5% material flow (compared to the original toolpath flow ratio). We investigated the effect of the ironing setting using Bambu Lab printers (models P1S and X1-Carbon) with a 0.40-mm nozzle at 0.20 mm layer height. Initially, the 35-mm static devices were printed with standard settings (100% flow ratio). These devices were tested using a solution of red dye, and they did not leak. Next, the "ironing" setting of the printer was enabled for all solid layers. This was used to print devices with 0% ironing flow (no material is used to retrace the toolpath; the heated nozzle retraces the toolpath). Other settings tested include printing devices with 5% and 10% ironing flow (where the nozzle retraces the toolpath with 5 or 10% of the original flow rate being dispensed). These static well devices were tested for leakage with the dye, and they also did not leak (Fig. 3). To investigate the density and area of the voids between layers, devices were dissected, and SEM micrographs were obtained and analyzed using ImageJ software. Figure 3a presents an SEM micrograph of standard printed devices with a corresponding void density estimated to be 7 void/mm^2 and the average void area being 1,302 µm^2. Devices printed with 0% ironing flow (Fig. 3b) resulted in a void density of 3 void/mm^2 (average void area = 272 µm^2). Devices made with 10% ironing flow produced very few voids that were difficult to find. The average void density was less than 1 void/mm^2 and the average void area that could be found was 33 µm^2 (Fig. 3c). A comparison of the average void area with the Bambu printed devices can be found in Fig. S4b. Interestingly, when the standard printed devices of the two printers were compared,

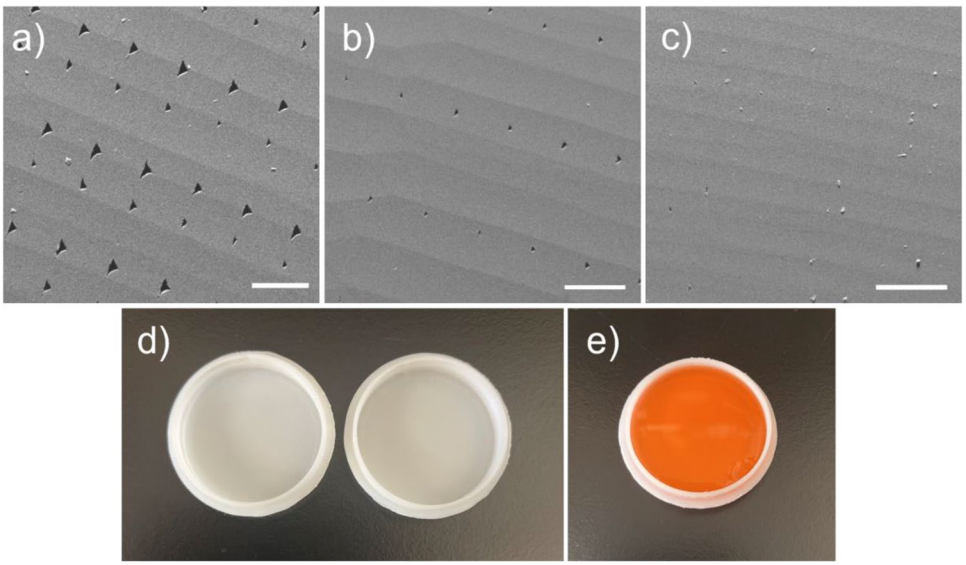

Fig. 3 Optimizing Bambu Lab printing parameters to fabricate leak-free static devices. **a** SEM micrograph of voids in between layers using standard printing parameters. **b** SEM micrograph of voids in between layers using 0% ironing flow. **c** SEM micrograph of voids in between layers using 10% ironing flow. **d** Printed devices in polystyrene (PS) materials. **e** Devices printed with the specified standard and ironing parameters showed no signs of leakage in static devices. Scale bar = 400 µm

it was found that the average void area from the Bambu printed devices was approximately ten times smaller than that of the Stratasys-printed devices. In addition, the optimized static settings with the Stratasys printer (− 0.0508 mm offset) yielded an average void area similar to that obtained with the standard Bambu print settings (without ironing). This gives confirmation as to why the Bambu standard printed devices were leak-free for static devices (however, as detailed below, these standard settings do lead to leakage with flow devices). The comparison data graphs in Fig. S4 also clearly show that the ironing feature results in a very small void area. One notable drawback associated with using the ironing feature is the increase in printing time, as indicated by the Bambu Studio slicing software. For instance, a standard printed fluidic device is estimated to print in 25 min compared to 58 min for printing with ironing enabled, regardless of the ironing flow percentage being used.

The surface roughness of these devices was also investigated using scanning electron microscopy (SEM). The results revealed that surface roughness is significant on devices printed with ironing enabled, especially when using the 5 and 10% ironing flow settings (Fig. S5). In addition, it is observed that increasing the ironing flow percentage also increases the sizes of grooves on the devices due to the materials being deposited during this process as the printer retraces the toolpath. We further investigated this effect using a 3D laser scanning microscope to measure the height of the grooves, which were found to be 23 µm for 0% ironing flow and 74 µm for 5% ironing flow devices. Devices with 10% ironing flow had grooves that measured up to 81 µm. The grooves can be observed with fluorescent imaging of stained cells in these static devices (Fig. S6).

Cell culture in static devices

The FDM-printed static culture devices (printed with PS) from both printers were characterized for biocompatibility with cell culture studies. These devices were compared to the use of PolyJet-based devices printed using VeroClear (VC). We have previously shown that cleaning with sodium hydroxide/sodium metasilicate solution is essential in culturing cells in these devices [3]. A side-by-side view of PS-based and VC-based 35-mm culture dish static devices is illustrated in Fig. 4a. Bovine pulmonary artery endothelial cells (BPAECs), which are commonly used to study vasodilation and red blood cell/endothelial cell interactions [35, 36], and Madin-Darby canine kidney cells (MDCK cells), which are commonly used in permeability screening methods [37, 38], were utilized to evaluate culturing of cells in these devices.

We characterized the devices, using MTT assays to assess the relative viability of cells between the PS-based (FDM printed) and VC-based (PolyJet printed) devices. MTT assay is a colorimetric assay that measures the metabolic activity of living cells by monitoring the reduction of MTT, which is yellow, to form formazan (purple) [33, 34]. In this study, two different cell lines, including BPAEC and MDCK cells, were employed (Fig. 4b and c). Cells were allowed to incubate for 24 h and 48 h before the MTT reagents were added, following the manufacturer's recommendations. Results were compared to 2 h of cell culture in the same device type. This was done so that a comparison could be made on cells growing and proliferating over time in each device relative to the 2-h time point. The relative absorbances were measured in each trial (24-h and 48-h cell cultures) by normalizing each absorbance to the absorbance measured in the 2-h cell culture devices. As a

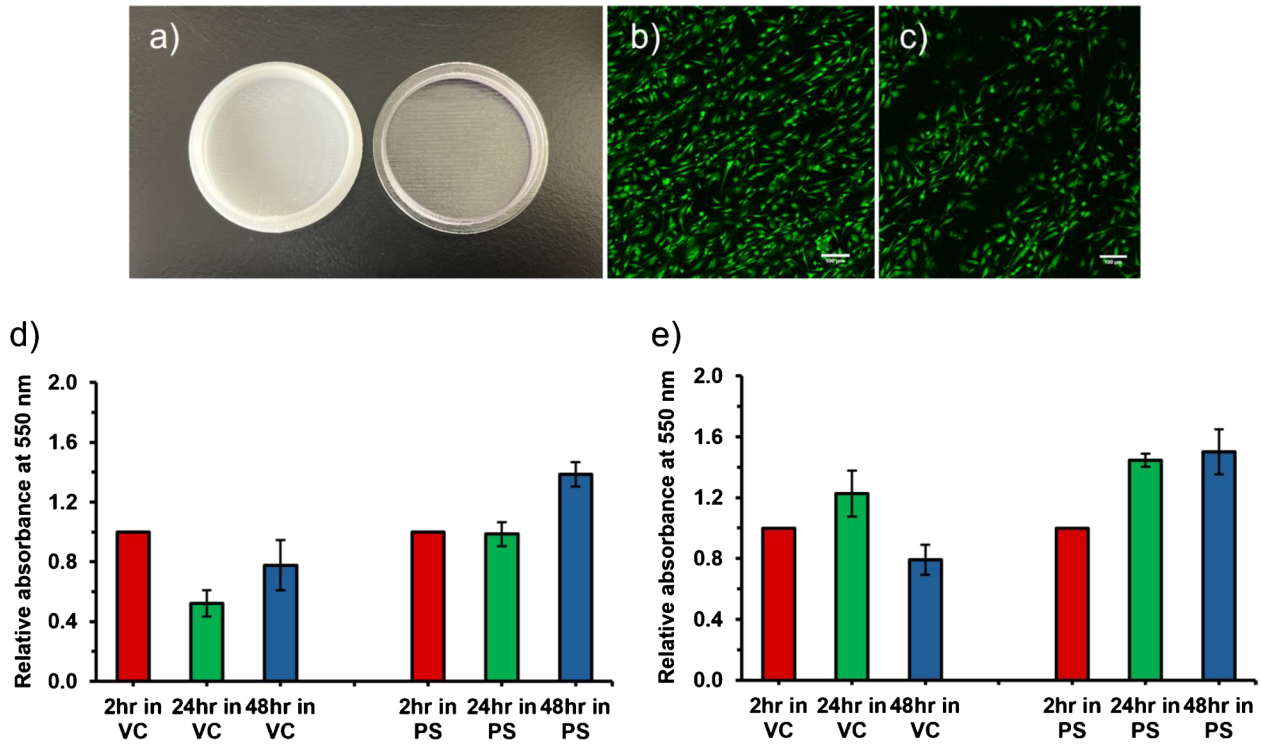

Fig. 4 **a** Side-by-side view of polystyrene (left) and VeroClear (right) printed devices. Fluorescence micrographs of BPAECs cultured directly on polystyrene (**b**) and VeroClear (**c**) devices for 24 h. Scale bar: 100 µm. **d** Viability results of MTT assays for BPAECs cultured in polystyrene (PS) and VeroClear (VC) devices for 24 h and 48 h ($n = 6$). **e** Viability results of MTT assays for MDCK cells cultured in PS and VC devices for 24 h and 48 h ($n = 3$). Cells cultured for 2 h served as the control (red). Error bars are displayed as standard error of the mean (SEM)

result, the 2-h culture device does not have any error bars. As can be seen in Fig. 4d and e, devices printed with PS materials showed significant increases in relative absorbance (viability) in both cell lines as a function of time. Cells cultured on VeroClear devices, while still present, did not increase in viability or cell growth over time. This shows that for these cell lines, the PS-based FDM-printed devices led to more cell growth and proliferation.

NMR spectroscopy analysis

Previous studies have investigated potential leachates from PolyJet devices [3]. With the PS-based FDM devices, proton (^{1}H) NMR was employed to also see if any PS material leaches into solutions placed in the devices after printing. NMR was chosen due to the high molecular weight of PS and its aromatic structure having bands that can be easily identified within a chemical shift range from 6 to 8 ppm. Because the material is a bulk polymer, a multiplet was observed in this region (see Fig. S7a).

Experiments were performed with HIPS standard solutions (with a concentration range from 50 to 250 µg/mL) in order to generate a calibration curve and determine the limit of detection (LOD). While the results of the calibration curve are shown in Fig. S7b, the LOD was determined to be 30 µg/mL. To determine leachates in the printed devices, 3 mL PBS was added to the devices and incubated for a 48-h period. A liquid–liquid extraction of the PBS sample was performed using methylene chloride, followed by evaporation and reconstitution in 1 mL of deuterated chloroform. Results of the analysis showed that there was no band correlating to the aromatic region of PS in the extracts (Fig. S7c), meaning that no detectable PS was found in the extracts (with the LOD being 30 µg/mL). In addition, 150 µg/mL HIPS was spiked in PBS followed by liquid–liquid extraction (with the above-mentioned approach), with a recovery of 99.87% being found.

Flow devices printed with Stratasys Fortus 250mc

In addition to printing static cell culture devices, the Stratasys printer was utilized to fabricate insert-based flow devices. The design of the device features the design which was previously reported by Chen et al., with slight modifications [4]. This design is of interest to our applications because it allows cells cultured on rectangular inserts to be placed in the device and shear to be introduced over the cells (Fig. 5a and b). Also, the insert can

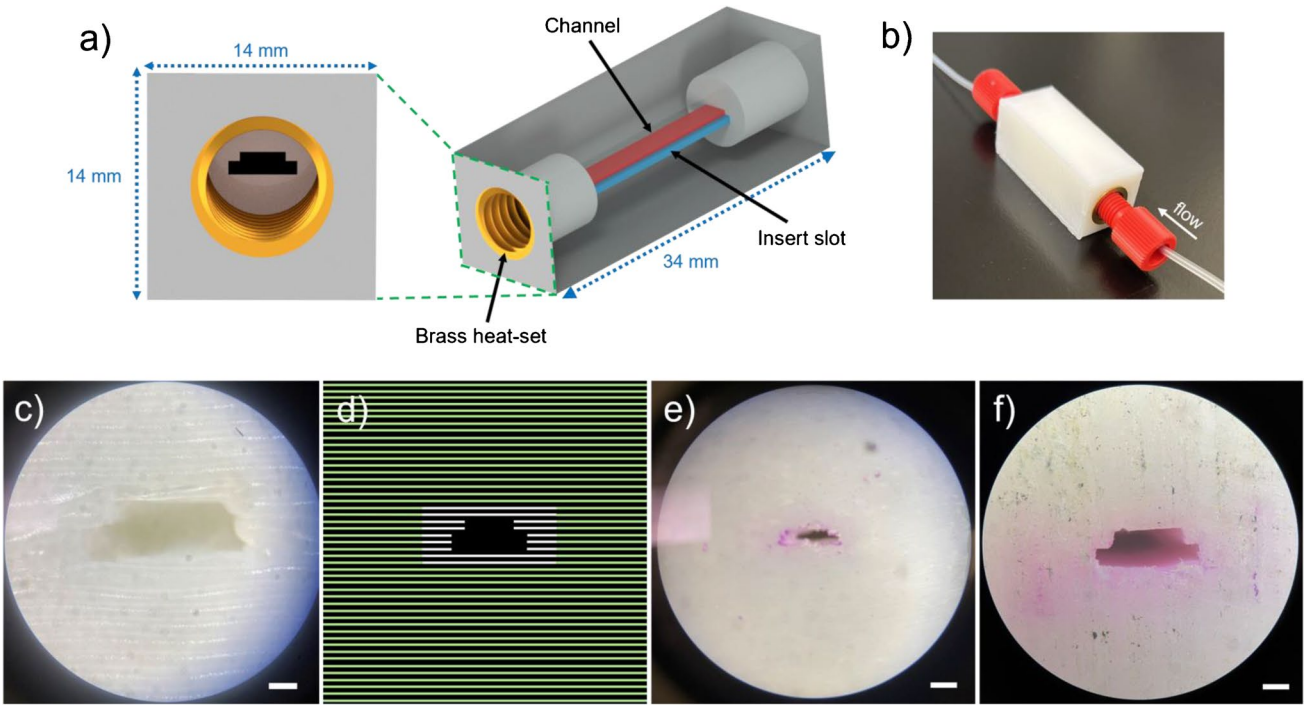

Fig. 5 Initial 3D-printed flow devices via Stratasys FDM printing approach. **a** CAD rendering of 3D-printed insert-based fluidic device. **b** Photograph of the assembled polystyrene–based device printed using standard printing parameters, with heat set inserts installed for commercially available threaded fluidic connections. **c** Cross-section of device printed with air gap − 0.0762 mm showed deformation of channels due to over-extrusion of printing materials. **d** Cartoon demonstrating the layers of the device within which different air gap values were utilized in the Stratasys printing process to achieve leak-free devices. White display layers around the channel and green for the bulk layers. **e** A micrograph showing devices printed with air gap − 0.0762 mm for two layers around the channel (white) and − 0.0254 mm for the bulk layers (green). **f** Micrograph of devices printed with air gap − 0.0254 mm for six layers around the channel (white) and − 0.0762 mm for the bulk layers (green), resulting in a device capable of cell culture studies. Scale bar = 100 µm

be removed easily for subsequent studies, including imaging and cell lysis. For the Stratasys printer, the air gap − 0.0508 mm, which successfully resulted in leak-free static devices, was used to print the devices after using standard print settings and − 0.0254-mm air gap value. Heat set inserts were installed in devices (with protocol described earlier, see Fig. S2) to allow the connection of tubing from devices to a pump. Devices were tested by continuously pumping a solution of Rhodamine B at a flow rate of 15 µL/min for 1 h. To observe leakage, the devices were dissected and examined under a stereo microscope. The results indicate leakage of flow devices (with air gaps − 0.0254 and − 0.0508 mm), as shown in Fig. S8. This is probably due to the pressure induced by the continuous introduction of fluid from the syringe pump, with the fluid finding a path within (and between) the print layers to leak through the devices. Another approach was to increase the negative air gap to − 0.0762 mm. This leads to the deformation of the channel as the excess materials change the channel shape (Fig. 5c).

To optimize the approach, devices were printed with varying negative air gap values that vary as a function of layers around the channel. Figure 5d illustrates the approach. We investigated this by assigning − 0.0762 mm air gap to a section (two layers each at the top and bottom of the channel) and − 0.0254 mm to the bulk layers away from the channel. This approach also resulted in the channel being somewhat deformed (Fig. 5e), but no leaking of the devices. In a similar study, − 0.0254 mm was assigned to six layers around the channels and − 0.0762 mm to the bulk layers. With these parameters, the channels were not deformed, and the devices were leak-free (Fig. 5f). Although there may be slight leakage to the layers immediately around the channel due to the air gap (− 0.0254 mm), this leakage was localized to that area and did not significantly impact the use of the devices for cell culture studies.

Flow devices printed with Bambu Lab

The Bambu Lab printers were also utilized to print the flow devices. The devices were tested following the aforementioned method of pumping 1 mM rhodamine B through the devices at a flow rate of 15 µL/min. Standard

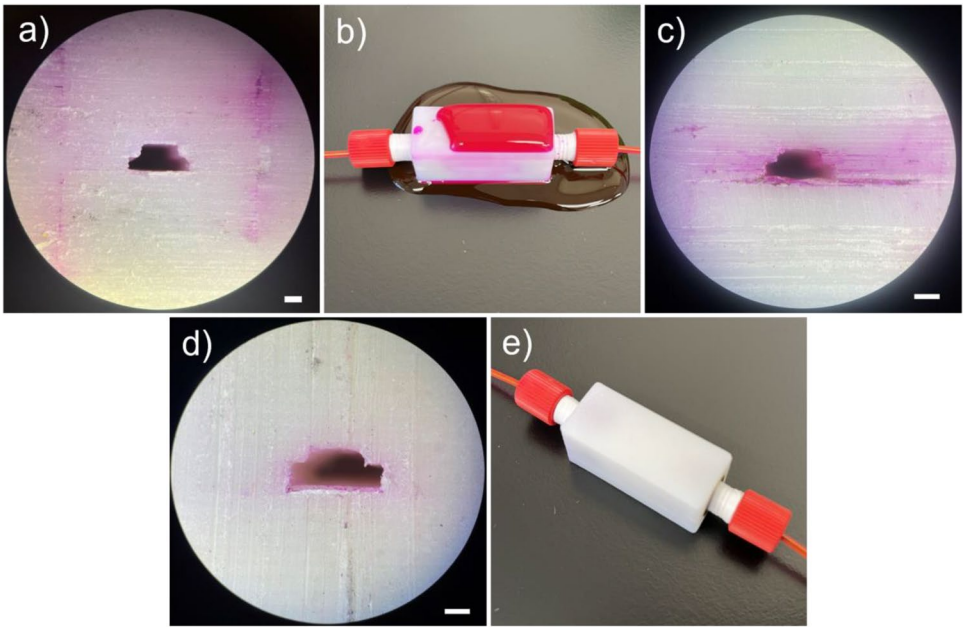

Fig. 6 Bambu Lab printed flow devices. **a** Cross-section of a standard printed device. **b** Assembled device printed with standard printing settings that leaked after a continuous flow of rhodamine B dye through the channel for 1 h. Micrographs showing leakage of a device printed with 0% ironing flow (**c**) and a leak-free device printed with 10% ironing flow (**d**). **e** Assembled device printed with 10% ironing flow, which did not leak when tested with a continuous flow of rhodamine B dye through the channel at 15 µL/min for 1 h. Scale bar = 100 µm

printing settings were initially used to print devices, and it was found that the devices leaked (Fig. 6a and b). While the size of voids with this setting did not lead to leakage with the static devices, when these same settings were used to print a flow device that was used with syringe pump-based flow, leakage through layers was clearly evident (Fig. 6b). We optimized the approach by printing devices with the ironing feature enabled. Different ironing flows, including 0, 2.5, 5, and 10%, were explored. With these devices, only the 10% ironing flow devices turned out to be leak-free (Fig. 6d). Moreover, the 10% ironing setting led to devices that did not leak with flow over the course of days (further times were not investigated). To further investigate this, we varied the flow rate from 15 to 1000 µL/min, yet the devices did not exhibit any signs of leakage (see Table S1 for a listing of the flow rates used and the resulting measured pressure). This can be explained by the extremely small voids with this print setting (average void area = 33 μm^2, see Fig. 3c). Figure S9 contains the results of devices printed with 2.5 and 5% ironing, respectively.

Cell culture in flow devices

The flow devices were characterized for biocompatibility through a flow-based cell culture study in which cells were immobilized on PS fibers. A comparative analysis between the PS-based FDM flow devices and VeroClear-based PolyJet flow devices was conducted [4]. PS nanofibrous 3D scaffolds were electrospun as described previously (Fig. S10) [32]. Integrating fibers into fluidic devices helps to better mimic the 3D extracellular matrix (ECM) that cells experience in vivo [4, 39]. The fibers were laser cut into rectangular inserts and sterilized. BPAECs were then seeded onto these inserts and incubated for 24 h. After 24 h, we performed a flow-based culture by placing some of the inserts into both flow devices (PS and VC-based) and immediately connected to a peristaltic pump that circulated media over the cells while in the incubator at 15 µL/min for 24 h (Fig. 7a). The remaining inserts in a petri dish were also incubated with new media for 24 h to serve as a static control. As seen in the micrographs found in Fig. 7b and c, both materials show similar results after 24-h culture with flow. Moreover, it is evident from Fig. 7d with the MTT assay results that both the FDM-based and PS-based devices were successful in culturing BPAECs under flow conditions.

Conclusion

In this work, we investigated the parameters that can be changed to create leak-free FDM-based microfluidic devices for use in cell culture. Stratasys Fortus 250mc and Bambu Lab P1S/X1-Carbon printers were utilized, with each printer being optimized based on different variables. Both static (dish) and flow-based cell culture devices were printed using PS material. The Fortus 250mc resulted in leak-free static devices when the toolpath was offset using an "air gap" value of − 0.0508 mm. Flow devices were also printed by assigning air gap values of − 0.0254 mm to six layers surrounding the channel and − 0.0762 mm to the bulk layer to maintain the channel shape of the devices. The Bambu Lab printed devices resulted in leak-free prints by optimizing the use of the "ironing" variable.

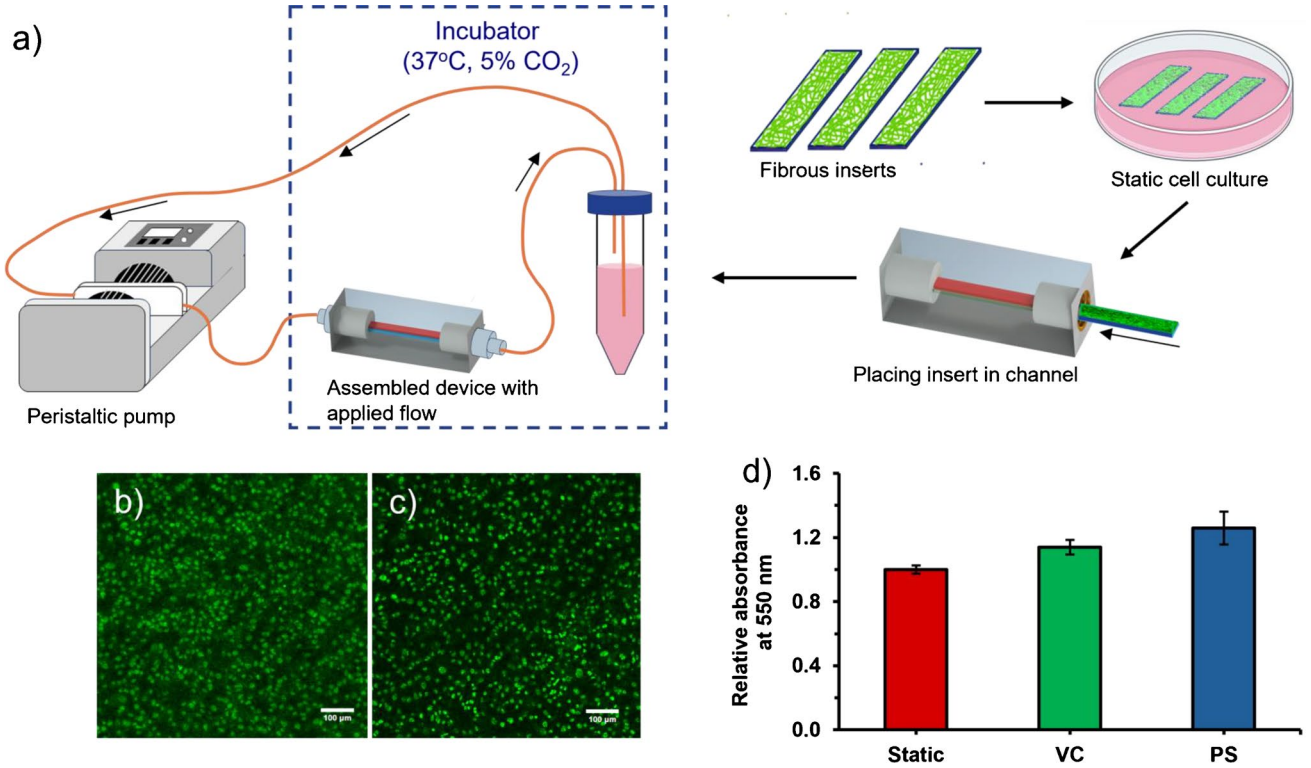

Fig. 7 **a** Schematic showing the process of creating an insert-based 3D-printed fluidic for 3D cell culture. Fiber-coated inserts are laser cut, and cells are seeded on them. The fibrous inserts can be easily assembled in a 3D-printed fluidic vessel that can be connected to downstream analytical modules. Fluorescence micrograph of BPAECs cultured directly on polystyrene (PS) fiber-coated inserts in PS printed devices (**b**) and VeroClear (VC) printed devices (**c**) after introducing flow over the cells for 24 h. **d** Viability results of MTT assays for BPAECs cultured under flow conditions in PS and VC devices for 24 h ($n = 5$). Cells cultured on PS fiber-coated inserts with no flow served as the control (red bar). Error bar = SEM

Successful static devices were printed with an ironing flow of 0, 5, and 10%; however, the only successful outcome regarding the printing of the flow devices was observed at 10% ironing flow. This setting led to the smallest void area of any of the tested parameters. Both printers were successful in fabricating devices capable of culturing viable endothelial and epithelial cells, including under flow conditions. NMR analysis showed no detectable leaching of PS from the devices. These results show that FDM printing can be a viable option (as compared to PolyJet printing) for creating leak-free microfluidic devices that can also be used for cell culture. This research lays the foundation for future studies in using flow-based FDM devices for cell culturing integrated with downstream analytical modules to study cell-to-cell communication.

Supplementary Information The online version contains supplementary material available at https://doi.org/10.1007/s00216-025-05958-1.

Author contribution Conceptualization: all authors. Methodology: all authors. Investigation, data curation, and formal analysis: Samuel Azibere and Michael Borovik. Writing—original draft preparation: Samuel Azibere. Writing—review and editing: all authors. Funding acquisition and project administration: R. Scott Martin.

Funding We received funding from the National Institutes of Health (NINDS, 2R01NS105888-06A1).

Data availability Data can be provided upon reasonable request to the corresponding author.

Declarations

Conflict of interest The authors declare no competing interests.

References

1. Bandak B, Yi L, Roper MG. Microfluidic-enabled quantitative measurements of insulin release dynamics from single islets of Langerhans in response to 5-palmitic acid hydroxy stearic acid. Lab Chip. 2018;18:2873–82.
2. Rothbauer M, Zirath H, Ertl P. Recent advances in microfluidic technologies for cell-to-cell interaction studies. Lab Chip. 2018;18:249–70.
3. Currens ER, Armbruster MR, Castiaux AD, Edwards JL, Martin RS. Evaluation and optimization of PolyJet 3D-printed materials for cell culture studies. Anal Bioanal Chem. 2022;414:3329–39.
4. Chen CP, Townsend AD, Hayter EA, Birk HM, Sell SA, Martin RS. Insert-based microfluidics for 3D cell culture with analysis. Anal Bioanal Chem. 2018;410:3025–35.

5. Cramer SM, Larson TS, Lockett MR. Tissue Papers: Leveraging Paper-Based Microfluidics for the Next Generation of 3D Tissue Models. Anal Chem. 2019;91:10916–26.
6. Chen C, Mehl BT, Munshi AS, Townsend AD, Spence DM, Martin RS. 3D-printed Microfluidic Devices: Fabrication, Advantages and Limitations-a Mini Review. Anal Methods. 2016;8:6005–12.
7. Nielsen AV, Beauchamp MJ, Nordin GP, Woolley AT. 3D Printed Microfluidics. Annu Rev Anal Chem. 2020;13:45–65.
8. Ligon SC, Liska R, Stampfl J, Gurr M, Mülhaupt R. Polymers for 3D Printing and Customized Additive Manufacturing. Chem Rev. 2017;117:10212–90.
9. Macdonald NP, Cabot JM, Smejkal P, Guijt RM, Paull B, Breadmore MC. Comparing Microfluidic Performance of Three-Dimensional (3D) Printing Platforms. Anal Chem. 2017;89:3858–66.
10. Konta AA, García-Piña M, Serrano DR. Personalised 3D Printed Medicines: Which Techniques and Polymers Are More Successful? Bioengineering. 2017;4:79–95.
11. Glasco DL, Sheelam A, Ho NHB, Mamaril AM, King M, Bell JG. Editors' Choice—Review—3D Printing: An Innovative Trend in Analytical Sensing. ECS Sensors Plus. 2022;1:010602.
12. Wang X, Huang L, Li Y, Wang Y, Lu X, Wei Z, et al. Research progress in polylactic acid processing for 3D printing. J Manuf Process. 2024;112:161–78.
13. Moradi M, Beygi R, Mohd, Yusof N, Amiri A, Da Silva LFM, Sharif S. 3D Printing of Acrylonitrile Butadiene Styrene by Fused Deposition Modeling: Artificial Neural Network and Response Surface Method Analyses. J Mater Eng Perform. 2023;32:2016–28.
14. Rohde S, Cantrell J, Jerez A, Kroese C, Damiani D, Gurnani R, et al. Experimental Characterization of the Shear Properties of 3D–Printed ABS and Polycarbonate Parts. Exp Mech. 2018;58:871–84.
15. Salentijn GIJ, Oomen PE, Grajewski M, Verpoorte E. Fused Deposition Modeling 3D Printing for (Bio)analytical Device Fabrication: Procedures, Materials, and Applications. Anal Chem. 2017;89:7053–61.
16. Gonzalez G, Roppolo I, Pirri CF, Chiappone A. Current and emerging trends in polymeric 3D printed microfluidic devices. Addit Manuf. 2022;55:102867.
17. Quero RF, Domingos da Silveira G, Fracassi da Silva JA, Pereira de Jesus, D. Understanding and improving FDM 3D printing to fabricate high-resolution and optically transparent microfluidic devices. Lab Chip. 2021;21:3715–29.
18. Castiaux AD, Spence DM, Martin RS. Review of 3D cell culture with analysis in microfluidic systems. Anal Methods. 2019;11:4220–32.
19. Kreß S, Schaller-Ammann R, Feiel J, Priedl J, Kasper C, Egger D. 3D Printing of Cell Culture Devices: Assessment and Prevention of the Cytotoxicity of Photopolymers for Stereolithography. Materials. 2020;13:3011.
20. Carve M, Wlodkowic D. 3D-Printed Chips: Compatibility of Additive Manufacturing Photopolymeric Substrata with Biological Applications. Micromachines. 2018;9:91.
21. Lerman MJ, Lembong J, Gillen G, Fisher JP. 3D printing in cell culture systems and medical applications. Appl Phys Rev. 2018;5:041109.
22. Ong LJY, Islam A, DasGupta R, Iyer NG, Leo HL, Toh YC. A 3D printed microfluidic perfusion device for multicellular spheroid cultures. Biofabrication. 2017;9:045005.
23. Anderson KB, Lockwood SY, Martin RS, Spence DM. A 3D printed fluidic device that enables integrated features. Anal Chem. 2013;85:5622–6.
24. Wang YI, Abaci HE, Shuler ML. Microfluidic blood-brain barrier model provides in vivo-like barrier properties for drug permeability screening. Biotechnol Bioeng. 2017;114:184–94.
25. Cenhrang K, Robart L, Castiaux AD, Martin RS. 3D printed devices with integrated collagen scaffolds for cell culture studies including transepithelial/transendothelial electrical resistance (TEER) measurements. Anal Chim Acta. 2022;1221:340166.
26. Ngan CGY, O'Connell CD, Blanchard R, Boyd-Moss M, Williams RJ, Bourke J, et al. Optimising the biocompatibility of 3D printed photopolymer constructs in vitro and in vivo. Biomed Mater. 2019;14:035007.
27. Rimington RP, Capel AJ, Player DJ, Bibb RJ, Christie SDR, Lewis MP. Feasibility and Biocompatibility of 3D-Printed Photopolymerized and Laser Sintered Polymers for Neuronal, Myogenic, and Hepatic Cell Types. Macromol Biosci. 2018;18:1800113.
28. Lu Z, Jiang X, Zuo X, Feng L. Improvement of cytocompatibility of 3D-printing resins for endothelial cell adhesion. RSC Adv. 2016;6:102381–8.
29. Warr C, Valdoz JC, Bickham BP, Knight CJ, Franks NA, Chartrand N, et al. Biocompatible PEGDA Resin for 3D Printing. ACS Appl Bio Mater. 2020;3:2239–44.
30. Selemani MA, Kabandana GKM, Chen C, Martin RS. 3D-Printed Microfluidic-Based Cell Culture System With Analysis to Investigate Macrophage Activation. Electrophor. 2025. https://doi.org/10.1002/elps.8109
31. Hayter EA, Castiaux AD, Martin RS. 3D-printed microfluidic device with in-line amperometric detection that also enables multi-modal detection. Anal Methods. 2020;12:2046–51.
32. Huang K, Castiaux A, Podicheti R, Rusch DB, Martin RS, Baker LA. A Hybrid Nanofiber/Paper Cell Culture Platform for Building a 3D Blood-brain Barrier Model. Small Methods. 2021;5:2100592.
33. Kumar P, Nagarajan A, Uchil PD. Analysis of Cell Viability by the MTT Assay. Cold Spring Harb Protoc. 2018;2018:https://doi.org/10.1101/pdb.prot095505.
34. Ghasemi M, Liang S, Luu QM, Kempson I. The MTT Assay: A Method for Error Minimization and Interpretation in Measuring Cytotoxicity and Estimating Cell Viability. In: Friedrich O, Gilbert DF, editors. Cell Viability Assays: Methods and Protocols. New York, NY: Springer US; 2023. p. 15–33.
35. Lockwood SY, Erkal JL, Spence DM. Endothelium-derived nitric oxide production is increased by ATP released from red blood cells incubated with hydroxyurea. Nitric Oxide. 2014;38:1–7.
36. Genes LI, Tolan NV, Hulvey MK, Martin RS, Spence DM. Addressing a vascular endothelium array with blood components using underlying microfluidic channels. Lab Chip. 2007;7:1256–9.
37. Irvine JD, Takahashi L, Lockhart K, Cheong J, Tolan JW, Selick HE, et al. MDCK (Madin-Darby Canine Kidney) Cells: A Tool for Membrane Permeability Screening. J Pharm Sci. 1999;88:28–33.
38. Bokulić A, Padovan J, Stupin-Polančec D, Milić A. Isolation of MDCK cells with low expression of mdr1 gene and their use in membrane permeability screening. Acta Pharm. 2022;72:275–88.
39. Chen CP, Mehl BT, Sell SA, Martin RS. Use of electrospinning and dynamic air focusing to create three-dimensional cell culture scaffolds in microfluidic devices. Analyst. 2016;141:5311–20.